Research Article

Xiaopei Guo, Tao Li*, Zhiqiang Shang, Yulin Zhu, and Guannan Li

The precipitation behavior of second phase in high titanium microalloyed steels and its effect on microstructure and properties of steel

https://doi.org/10.1515/htmp-2022-0027
received February 07, 2022; accepted February 25, 2022

Abstract: The thermodynamic precipitation behavior of the second-phase particles in Nb-containing high titanium microalloyed steel has been studied by calculation in this article. It is revealed that FCC_A1#2 is isomorphic with FCC_A1#3 and the contents of Ti and Nb elements are much higher than that of FCC_A1#3. The influence of different quenching temperatures on microstructure and mechanical properties of steel was also studied. The results indicate that the quenching temperature should be controlled below 1,100°C and the soaking time should not exceed 60 min to avoid abnormal grain growth. The thermodynamic calculation and experimental results have certain theoretical guiding significance for the practical industrial application of high titanium–niobium steel.

Keywords: precipitation behavior, microalloyed steels, impact toughness

1 Introduction

High strength steels are used in many fields, especially in automobiles. In recent years, the microalloyed steels, in which microalloy elements of niobium (Nb), vanadium (V), titanium (Ti), molybdenum (Mo), and so on are added in, have been extensively studied for its excellent mechanical properties and the reduction in weight [1–3]. The addition of alloying elements to steel can precipitate fine carbonitride, resulting in precipitation strengthening [4]. On the other hand, these precipitates can be nailed at grain boundaries to refine grains, thus improving the strength. It is generally thought that Nb is the most effective microalloy element which retards the recrystallization process of steel. It is reported that mechanism of reducing the grain size by Nb is mainly attributed to two factors [5,6]. The first is that the fine niobium carbide (NbC) precipitates can pin the interface of grain growth after recrystallization [7]. The second is that the Nb atoms dissolved in the steel have a drag effect on grain boundary migration. The Nb–Ti microalloyed steel is a common microalloyed steel which generally adopts the combination of high Ti and low Nb due to the economy of Ti resources. The size and quantity of the precipitates in the steel and the microstructure after rolling can be controlled by thermo mechanical control process (TMCP) in the industrial production of Nb–Ti steel, which can improve the strength of the steel [8,9].

Many researchers elucidated the Nb–Ti microalloyed steel from different aspects, such as the influence of different contents of Nb and Ti, the species of precipitates, and the change in heat treatment on the properties and microstructure of the steel. Zhou and Priestner [10] investigated the evolution of precipitates in Nb–Ti microalloyed steel during solidification and cooling process and found that precipitation of carbonitrides was strongly associated with the precipitation of manganese sulfide (MnS). Ma et al. [11] found that the precipitates formed a chain-like distribution along the austenite gain boundary at low cooling rate and few microalloying elements precipitate at high cooling rates. Grajcar [12] analyzed the precipitation process in Nb–Ti microalloyed Si–Al TRIP steel by thermodynamic calculation and found that silicon play a decisive role in reducing the solubility of MX-type phases in austenite of the steel, while Mn increases the solubility of micro additions and metalloids.

* **Corresponding author: Tao Li,** College of Metallurgy and Energy, North China University of Science and Technology, 063000, P. R. China, e-mail: litao@ncst.edu.cn
Xiaopei Guo, Zhiqiang Shang, Yulin Zhu: College of Materials Science and Engineering, Chongqing University, Chongqing, 400044, P. R. China; Chongqing Key Laboratory of Vanadium-Titanium Metallurgy and Advanced Materials, Chongqing University, Chongqing, 400044, P. R. China
Guannan Li: College of Materials Science and Engineering, Chongqing University, Chongqing, 400044, P. R. China; Technical Center, Handan Branch of Hegang Co., Ltd, Handan, 056015, P. R. China

It is well recognized that the composition, cooling rate, heat treatment, and deformation of the microalloyed steel affect the size, type, and distribution of second-phase particles and then change the microstructure and mechanical properties [13–16]. The grains that are in the metastable state will grow up and coarsen under the action of high temperature. However, the large grain size has a serious deterioration effect on the strength, toughness, fatigue strength, and other properties of steel [17–20]. The austenitizing temperature and soaking time, as the most critical parameters in the heat treatment process, seriously affect the size and distribution of austenite grains and the degree of solid solution of microalloying elements [21–25]. Therefore, it is important to investigate the growth process of austenite grain, which is helpful for enterprises to develop a reasonable casting billet heating process, subsequent heat treatment process, and obtain good performance of products. In the current work, the precipitation behavior of different phases in the hot-rolled Nb–Ti steel in balanced cooling process conditions is calculated by using Thermo-Calc software. The austenite grains and the microstructure of the steel treated by different heat treatment process were observed by optical microscopy (OM) and scanning electron microscopy (SEM). In addition, the low temperature impact toughness and Vickers hardness were detected under different quenching and tempering processes, which are associated with the microstructure.

2 Experiment

2.1 Materials and process

Table 1 shows the composition of the steel in which the Ti content is 0.10%, while the Nb content is relatively low at 0.025%. The steel was produced by converter smelting followed by the ladle furnace refining, vacuum refining, and continuous casting. Then, the billets were heated and held in a furnace that had been heated up to 1,250 ± 20°C for a certain period of time before being rolled to produce steel plates.

A number of samples with the dimensions of 13 mm × 13 mm × 65 mm and 10 mm × 10 mm × 5 mm were machined by electro-spark wire-electrode cutting from the steel plates. The samples with the size of 10 mm × 10 mm × 5 mm were quenched at a series of temperatures of austenitization. As shown in Figure 1(a), the quenching temperatures were 900, 1,000, 1,100, 1,150, 1,200, and 1,250°C, respectively, and the holding time was different from 20 min to 80 min for the research of the effect of heat treatment process on austenite grain size. Subsequently, in order to study the effects of different quenching temperatures on impact properties and microstructure, samples with the dimensions of 13 mm × 13 mm × 65 mm were quenched at different temperatures (860, 900, 940, 980 and 1,020°C) and tempered at 550°C for 60 min. The heat treatment schematic is shown in Figure 1(b). Then, the samples treated with various heat treatments were processed into 10 mm × 10 mm × 55 mm V-notch standard samples for their low temperature impact properties test.

2.2 Mechanical property

Charpy V-notch impact test at –20°C were conducted assisted by liquid N cooling on a metal pendulum impact tester to evaluate the mechanical properties of the samples after heat treatment. Three samples were tested for each heat treatment process to ensure the reliability of the data. Meanwhile, Vickers hardness tests were performed at eight different locations on each sample and took the average as final results of micro hardness.

2.3 Microstructure characterization

The samples for observing austenite grains were cut along the middle parts that have undergone heat treatment under different conditions. Then, the observed surface of the samples was ground by sandpaper and polished to a mirror by diamond spray. The samples were placed in a mixture of saturated picric acid aqueous solution, a small amount of corrosion inhibitor and a small amount of hydrochloric acid, and the water bath hot etching was

Table 1: Chemical composition of Nb–Ti composite microalloyed steels (wt%)

Elements	C	Si	Mn	P	S	Nb	Ti	Als	Ca	N
Content	0.075	≤0.10	≤1.25	≤0.012	≤0.002	0.025	0.10	0.025	0.003	<0.005

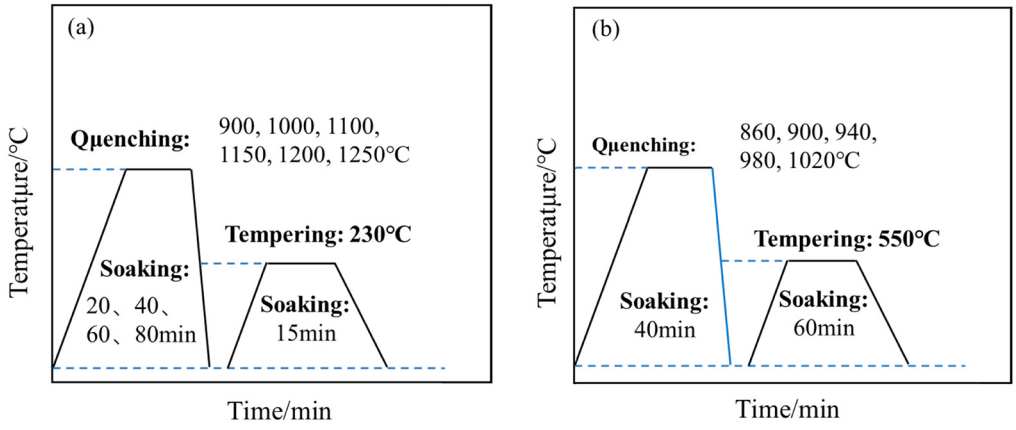

Figure 1: Different heat treatment regimes in the experiment: (a) schematic diagram of austenite grains sample treatment process and (b) different quenching processes for the impact tests.

carried out to show the grain boundaries of the austenite grains of the samples under different processes in a certain temperature range (60–80°C). At the same time, the original austenite grain morphology of the corroded samples was observed by using an inverted microscope (Zesiss Axio Vert. A1), and ten metallographic photos with different magnifications were collected. The transversal method was used to analyze the austenite grains of samples under different heat treatment processes, and the average grain size was calculated. The statistical number of grains of a single sample was no less than 300.

The samples that have undergone different quenching processes for the impact test were grounded by sandpapers and polished by diamond polishing spray. The 4 vol% nital was used to etch the surface of the polished samples in order to reveal the evolution of the microstructure. The microstructure was characterized by OM and SEM.

3 Results and discussion

3.1 Thermodynamics analysis of the second-phase particles

The equilibrium phase diagram of the experimental steel within the temperature range of 200–1,600°C was calculated by Thermo-Calc software. The relationship between the second-phase precipitation content and temperature is shown in Figure 2. The temperature was between 200–1,600°C, mainly because the smelting temperature of steel is generally 1,600°C, and the possible particles in the steel have been precipitated when it is cooled to 200°C. In order to more directly reflect the specific precipitation amount of the second phase, the logarithmic ordinate was adopted. It can be seen from Figure 2 that the second phase precipitated in the equilibrium cooling process of the experimental steel in the order of precipitation temperature mainly includes $Ti_4C_2S_2$, FCC_A1#3, FCC_A1#2, MNS, Cementite, $M_2P\_C_{22}$, M_5C_2, $M_{23}C_6$, and M_7C_3, among which $Ti_4C_2S_2$, Cementite, M_5C_2, and M_7C_3 are transition precipitates and exist only in a certain temperature range. FCC_A1#2, FCC_A1#3, and MnS precipitate stably in a wide temperature range.

In order to clarify the elements and contents of each phase, the variation in the content of each element in each phase with the precipitation temperature was calculated, as shown in Figure 3. The statistical analysis was

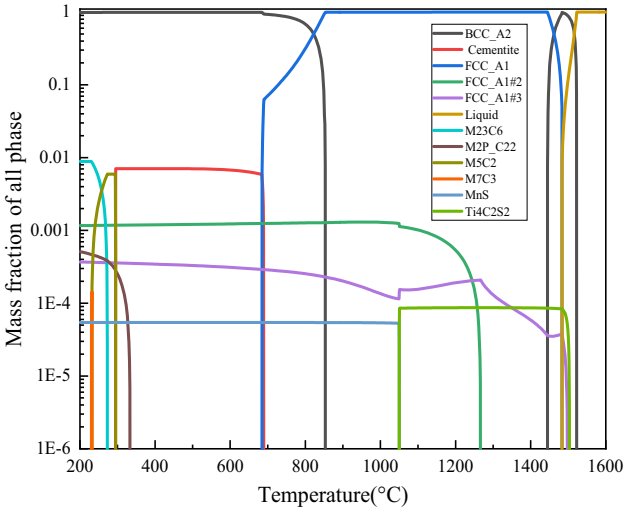

Figure 2: Relationship between the precipitation of the second phase and temperature.

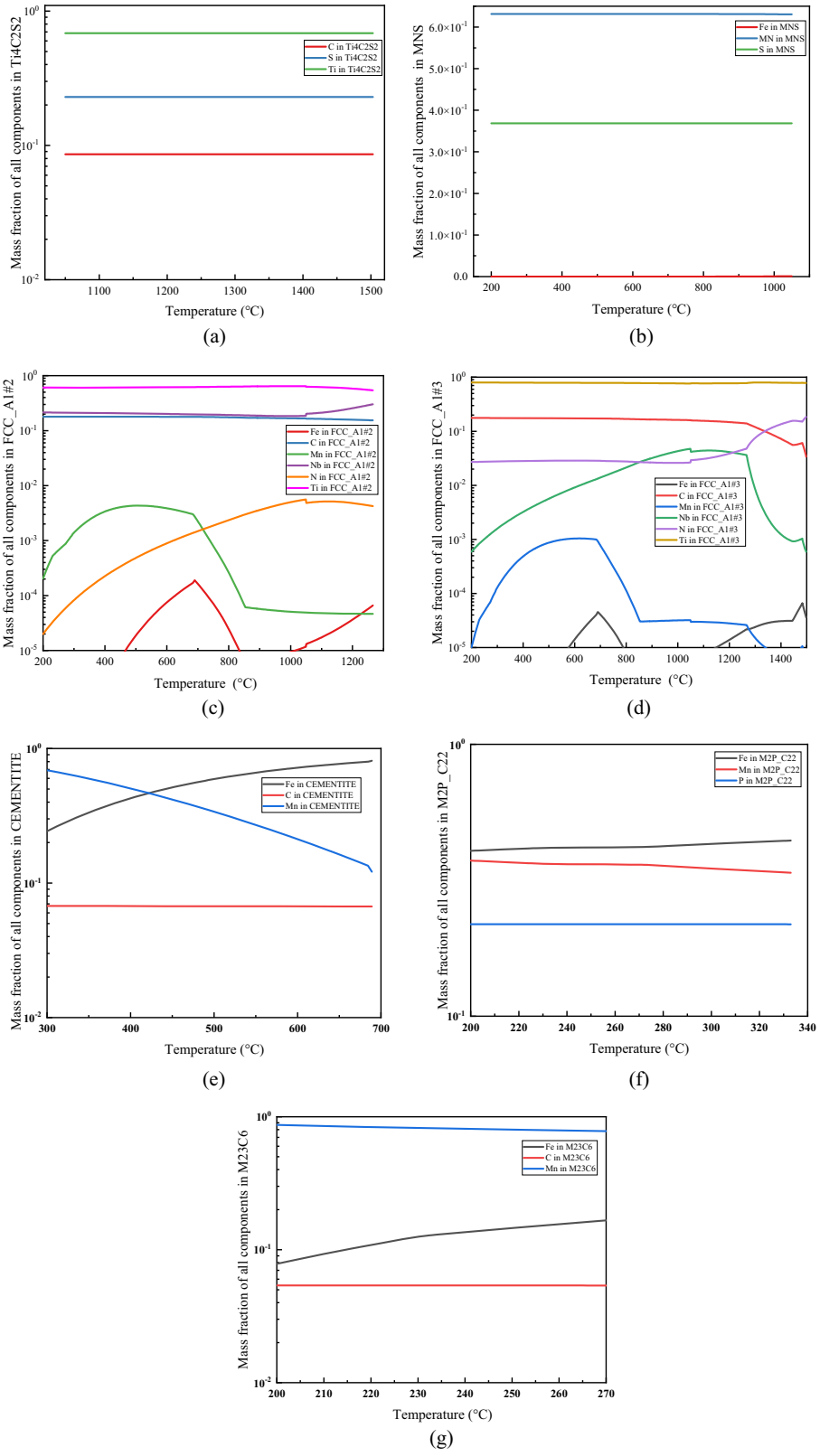

Figure 3: The relation between the composition ratio of each precipitated phase and temperature in experimental steel: (a) $Ti_4C_2S_2$, (b) MnS, (c) FCC_A1#2, (d) FCC_A1#3, (e) cementite, (f) $M_2P\_C_{22}$, and (g) $M_{23}C_6$.

carried out on all kinds of second-phase precipitation by Thermo-Calc, as shown in Table 2, which mainly includes the maximum precipitation mass fraction, initial formation temperature, complete decomposition temperature, etc.

Based on the comprehensive analysis of the data in Figures 2 and 3 and Table 2, it can be known that the liquidus temperature of the experimental steel is 1,522°C. $Ti_4C_2S_2$ phase began to precipitate at about 1,503°C in the solid–liquid two-phase zone, and the precipitate amount rose sharply to a certain extent after the temperature was lowered by about 50°C, and the precipitate rate became slow. At about 1,266°C, the maximum precipitate amount was about 8.68×10^{-5}. When the temperature dropped to about 1,049°C, almost all of the $Ti_4C_2S_2$ precipitate disappeared. It can be seen that the contents of constituent elements Ti, C, and S in the phase are basically not affected by temperature. $Ti_4C_2S_2$ phase is a transition phase, and its precipitation at high temperature can play the role of pinning austenite grain boundary and combining S element in the steel matrix, reducing the precipitation amount of MnS at high temperature, so as to weaken the adverse effect of MnS precipitates on the rolling process.

FCC_A1#3 begins to precipitate at about 1,498°C, that is, in the solidification stage of molten steel. The precipitate amount of FCC_A1#3 first increases rapidly, then decreases in a small range around 1,450°C, and then continues to rise and reaches a small peak at about 1,266°C. At this time, FCC_A1#2 begins to precipitate. The content of $Ti_4C_2S_2$ and FCC_A1#3 phase began to decrease, but the decrease in $Ti_4C_2S_2$ phase is not obvious. When the temperature drops to about 1,049°C, that is, the decomposition temperature of $Ti_4C_2S_2$ phase, the content of FCC_A1#3 phase suddenly decreases, and then increases slowly. The reasons for the change in FCC_A1#3 phase content during this period of temperature are investigated in detail. The first decrease may be due to the rapid transformation of high-temperature ferrite to austenite. The solubility product of the constituent elements of FCC_A1#3 phase in the matrix phase became larger, leading to its diffusion into the matrix and the decrease in phase content. The second decrease may be due to the fact that FCC_A1#3 phase is mainly used as nucleation particle after phase FCC_A1#2 begins to precipitate, and the structure of FCC_A1#2 phase is the same as that of FCC_A1#3 phase, leading to the transfer of some elements to the new phase FCC_A1#2. According to Figure 3(d) and Table 2, the main elements in the FCC_A1#3 phase include Ti, C, N, Nb, a small quantity of Fe and Mn, etc. The maximum content of Nb element in the FCC_A1#3 is also two orders of magnitude lower than that of Ti, so it can be considered that the FCC_A1#3 phase is mainly composed of Ti(C, N). In the precipitation process of FCC_A1#3, Ti elements account for about 80% . In the early stage, the account of N elements is larger than that of C elements, which illustrated that main precipitation form is TiN in the high temperature. Ti(C, N) becomes the main precipitation and contains a trace amount of Nb element with the decrease in temperature and the consumption of N element and the increase in C activity in steel. This is because Ti(C, N) particles which serve as nucleation in the steel matrix promotes the precipitation of Nb(C, N).

FCC_A1#2 phase rapidly precipitates from about 1,266°C and reaches a maximum precipitate amount of 1.31×10^{-3} at 956°C. Then, its amount decreases slowly, but the overall change is not significant. According to Figure 3(c), it can be seen that N element only partially precipitates at the beginning, and then the proportion of N element in FCC_A1#2 phase becomes lower and lower, while the

Table 2: The results of equilibrium precipitation of the second-phase particles in experimental steel

Phase of precipitation	Maximum precipitation mass fraction	Maximum precipitation temperature/°C	The temperature of starting to precipitate/°C	The temperature of complete decomposition/°C
$Ti_4C_2S_2$	8.68×10^{-05}	1266.90	1503.28	1049.25
FCC_A1#3	3.69×10^{-04}	—	1498.06	—
FCC_A1#2	1.31×10^{-03}	956.00	1266.90	—
MnS	5.43×10^{-05}	—	1050.80	—
Cementite	7.05×10^{-03}	430.00	689.82	294.15
$M_2P\_C_{22}$	5.11×10^{-04}	—	333.72	—
M_5C_2	5.93×10^{-03}	294.15	295.06	232.14
$M_{23}C_6$	8.84×10^{-03}	230.57	273.11	—
M_7C_3	1.44×10^{-04}	232.14	232.14	230.57

Note: The temperature range calculated for the second-phase precipitation is 200–1,600°C. "—" means that the precipitated phase has no decomposition behavior within the calculated temperature range or precipitates to 200°C.

proportion of Nb element increases rapidly after the initial precipitation, and gradually stabilizes with the decrease in the temperature. It can be seen that the content of C is much larger than that of N, so it is believed that FCC_A1#2 is mainly composed of (Ti, Nb)C. Since the FCC_A1#3 and FCC_A1#2 are isomorphic, part of N elements may be replaced by C elements in the precipitation process.

After the complete decomposition of $Ti_4C_2S_2$, S element is liberated, and a large number of MnS are precipitated in a very small temperature range, as shown in Figure 3. As the temperature decreased, MnS is continuously precipitated, with a precipitation amount of about 5.43×10^{-5}, and the proportion of elements in the phase almost remained unchanged.

Cementite is mainly composed of C, Fe, and Mn elements. The Cementite begins to precipitate at about 689°C and then completely decomposes at about 294°C. $M_2P\_C_{22}$ phase consists of P, Fe, and Mn elements, which is a kind of phosphide. It is a low-temperature precipitated phase, which begins to precipitate in ferrite at about 333°C. It can be ignored due to the extremely low P content in steel and the large difference between the precipitation temperature of $M_2P\_C_{22}$ phase and the actual production temperature of steel.

The precipitates of M_5C_2, $M_{23}C_6$, and M_7C_3 are all carbides, which can be expressed as (Fe, Mn)C, and the precipitation temperatures of the three phases are quite close, which are 295, 273, and 232°C, respectively. The M_5C_2 and M_7C_3 only precipitate and dissolve at a small temperature range. The $M_{23}C_6$ has a positive effect on steel strengthening that precipitates in chain shape at grain boundary [26,27].

3.2 Effect of second-phase particles on austenite grains

The average austenite grain size of the experimental steel under different quenching temperatures and soaking times, obtained by using the transversal line method, are shown in Table 3 and Figure 4. It can be seen that the average austenite grain size of experimental steels with different holding time almost increases exponentially with the increase in the quenching temperature. Figure 5 shows the austenite grain morphology obtained after holding uniformly for 40 min at different quenching temperatures. It is clear that the austenite grain size gradually increases with the increase in quenching temperature. When the quenching temperature is between 900–1,000°C, the size of austenite grains is more small, whose size distribution is uniform. However, the grain growth trend is not obvious with the temperature, and it is difficult to judge the degree of its growth only by preliminary observation. It can be seen from Table 3 that the average austenite grain sizes at 900 and 1,000°C are about 3.4 and 8.7 μm, respectively. It is obviously observed from Figure 5(c) and (d) that the number of austenite grains decreases significantly and the average grain size increases to a considerable extent. In addition, the microstructure of mixed grain (mixed grain refers to the large difference in austenite grain size) has a serious impact on steel strength and toughness. However, it can be observed from Figure 5(e) and (f) that abnormally coarse austenite grains are equiaxed, and their average size is as large as about 70 μm, when the quenching temperature reaches 1,200–1,250°C.

Table 3: Average grain size of austenite under different process conditions

Temperature/°C		Holding time/min			
		20	40	60	80
Average grain size/μm	900	2.92	3.41	4.16	4.73
	1,000	7.20	8.69	10.79	12.19
	1,100	13.69	16.98	19.15	22.34
	1,150	21.88	26.21	31.45	37.46
	1,200	30.32	40.43	47.52	51.77
	1,250	44.53	51.27	64.32	74.22

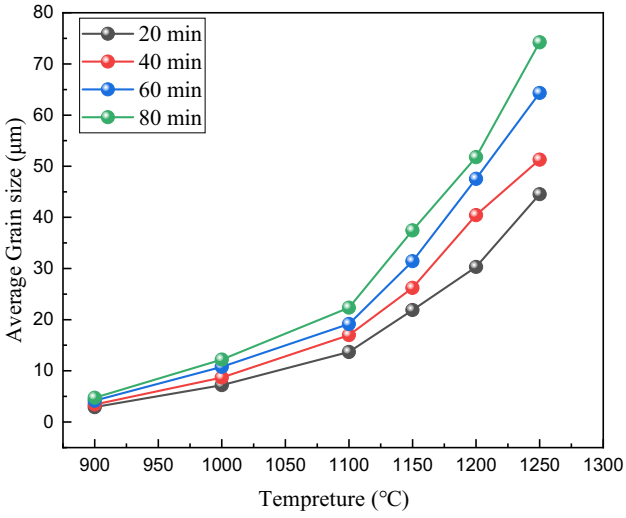

Figure 4: The relationship between average austenite grain size and temperature of experimental steels.

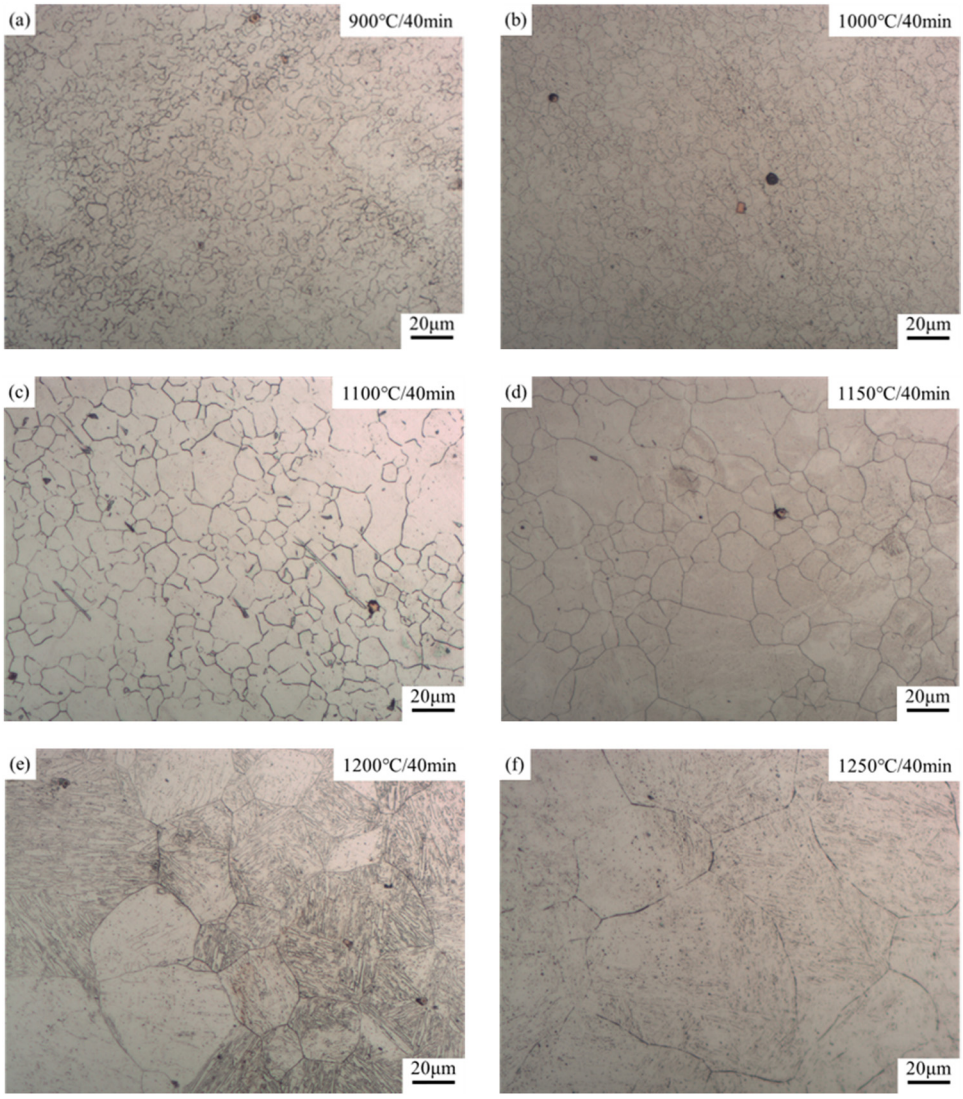

Figure 5: The austenite grain morphology after holding for 40 min at different quenching temperatures: (a) 900°C, (b) 1,000°C, (c) 1,100°C, (d) 1,150°C, (e) 1,200°C, and (f) 1,250°C.

The austenite grain growth process is actually the coupling effect of element diffusion, thermal activation, and interface migration. The austenitic grain boundary realizes migration with the driving force of the interface energy. The effect of quenching temperature on the grain growth is mainly reflected in the diffusion rate of atoms at the grain boundary. The variation in austenite grain growth rate under the same soaking time is generally calculated by equation (1).

$$\upsilon = \frac{k\alpha[\exp(-Q/RT)]}{d}, \quad (1)$$

where k is a constant, α represents grain boundary interface energy ($J{\cdot}mol^{-1}$), Q represents the activation energy ($J{\cdot}mol^{-1}$), R represents gas equilibrium constant of 8.314 $J{\cdot}(mol \times K)^{-1}$, T represents absolute temperature (K), and d represents average austenite grain size (μm). It can be seen from equation (1) that when the soaking time is consistent, the grain growth rate increases with increase in the temperature. The migration rate of grain boundary would be reduced by fine second-phase particles including FCC_A1#3, FCC_A1#2, and MnS, which are dispersed in the steel at the quenching temperature of 900–1,000°C. The second-phase particles that originally existed at grain boundary and played a role in pinning the grains are in metastable state and some of them begin to dissolve or coarsen with the increase in the quenching temperature, which finally lead to the weakening of the pinning force. Moreover, the increase in the temperature also increases the diffusion rate of atoms at grain boundary, which resulted in the rapid growth of austenite grains. The average grain size of austenite increases sharply at the

quenching temperature up to 1,250°C, which is due to a large number of decompositions of FCC_A1#2 phase that occupies the largest mass fraction of the second-phase particles in the steel, resulting in the severely weakened nailing effect. The reduction in total area of grain boundary decreases the interface energy, which makes the internal system more stable. That is the internal reason for the reduction in the number of austenite grain. Therefore, the actual quenching temperature should be controlled within 1,100°C in the heat treatment process of the experimental steel.

As shown in Table 3 and Figure 4, the number of small austenite grains decreases gradually and the average grain size increases at a slow rate with the increase in soaking time. When the soaking time increased from 20 min to 80 min, the average grain size increased only by 9 μm from about 13 μm. It can be seen that the soaking time has much less effect on the austenite grains than the quenching temperature. This is because most of the second-phase particles still exist at grain boundaries at this temperature, and the austenite grains can only keep the system stable by reducing the higher grain boundary energy caused by the grains inhomogeneity. The decrease in grain boundary energy leads to the outward migration of grain boundaries. Thus, the soaking time in the heat treatment process should not be too long.

3.3 The influence of quenching temperature on microstructure evolution

In the above discussion, it is known that the quenching temperature should be below 1,100°C. In order to ensure the proper grain size and solid solubility of microalloying elements in austenite, the quenching process route, as shown in Figure 1(b), was developed to explore the influence of quenching temperature on microstructure and properties. Three identical experimental steel samples were made in each process to ensure the accuracy of subsequent low-temperature impact toughness test results. The samples were tempered at 550°C to reduce the quenching stress for improving the comprehensive mechanical properties, which aim to fully precipitate the microalloying element carbides and reinforce steel matrix.

Figure 6 shows the SEM image of microstructure of the experimental steel treated by quenching at different temperatures for 40 min and tempering at 550°C for 60 min. It can be seen that the microstructure of the experimental steel changed significantly with the increase in quenching temperature. The microstructure is mainly granular bainite (GB) when the quenching temperature is 860°C, as shown in Figure 6(a). In addition, different sizes and morphology of carbides which are shown as the bright white point in the SEM exist in the GB matrix and grain boundary, which are sphere and short rod shaped. The offwhite lumps shown in the red circle are typical martensite/austenite (M/A) islands, whose morphology is not the same due to the differences in the decomposition rate and degree. The internal structure of M/A may be a mixture of two or more phases, such as martensite, ferrite, RA, bainite, etc. The main microstructure is still GB at the quenching temperature of 900°C, as shown in Figure 6(b). However, the length of massive block bainitic ferrite in GB decreased, and the GB is more uniform. In addition, few lath bainitic ferrites are observed in Figure 6(b). As the quenching temperature increases to 940°C, it can be seen from Figure 6(c) that the number and volume of bainite ferrite significantly decreases, and many slender lath bainite ferrite appears, with granular precipitates distributed between the lath. At the quenching temperature of 980°C, the width of lath bainite ferrite increases and the outline becomes clearer. Moreover, the number of fine white pointlike precipitates increases sharply and is generally distributed at the boundary of grains. When the quenching temperature is further increased to 1,020°C, the original austenite grain boundary can be clearly identified, as shown in Figure 6(e). The number of lath bainite ferrite increases and grows parallel to the grain boundary. The main reason for the evolution of the microstructure in the experimental steel is that the second-phase particles in the hot rolled steel dissolve with the increase in the quenching temperature, and the austenite whose grain size gradually increases becomes more stable. In the subsequent tempering process, the elements of the microalloyed steel are redistributed and combined, and a large number of nanometer carbides are precipitated in the steel.

3.4 The influence of quenching temperature on mechanical properties

The experimental steel samples treated with different quenching processes were cut into standard Charpy impact test specimens. Some of the impact test samples were made for metallographic specimen after grinding and polishing which were used to measure Vickers hardness by the HV-5 Vickers hardness instrument. Each sample

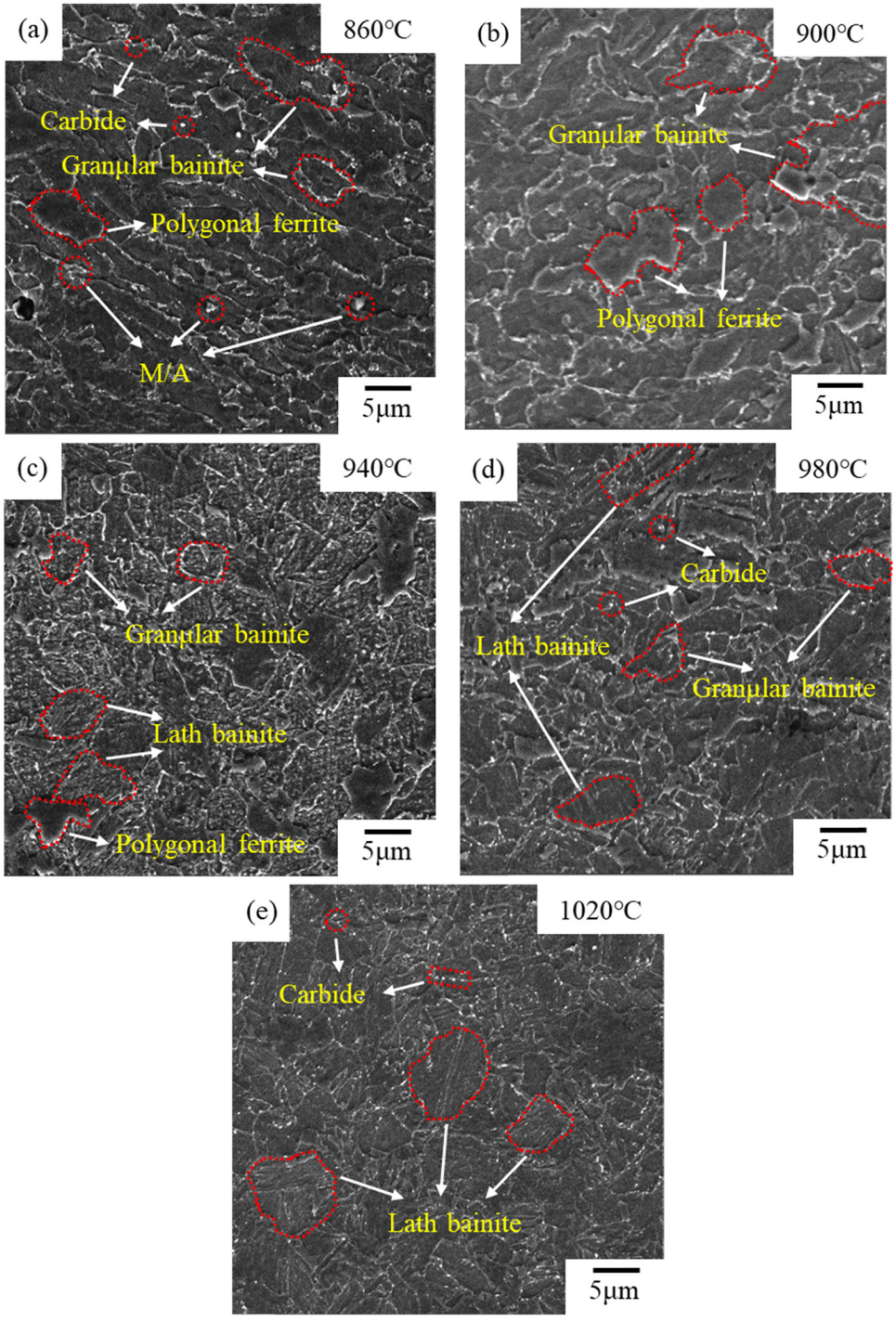

Figure 6: The SEM morphology of experimental steel at different quenching temperatures: (a) 860°C; (b) 900°C; (c) 940°C; (d) 980°C; and (e) 1,020°C.

was tested at 8 points with a holding of 10 s. The test results are shown in Table 4 and Figure 7.

It can be seen from Figure 7 that the impact toughness of the experimental steel fluctuates greatly with the quenching temperature which is much larger than the control standard of 48 J for the steel. The impact work value of the sample after 900°C quenching is as high as 300 J. The cause for the impact energy change in the experimental steel can be explained by its microstructure evolution. The granular bainite is the main microstructure after 860°C quenching and 550°C tempering. The block bainite ferrite which is the main matrix of the GB

Table 4: Low temperature impact energy and microhardness of experimental steels at different quenching temperatures

Quenching temperature/°C	Hardness, HV	Impact energy/J
860	189	264
900	191	299
940	212	297
980	224	243
1,020	244	280

has a higher dislocation density than the lath bainite ferrite. The distribution of spherical second phase and M/A structure in the matrix can effectively prevent the further propagation of the crack and reduce the stress concentration. The impact energy is significantly increased with the increase in the quenching temperature to 900°C for the higher overall homogeneity of the GB structure. The microstructure is still GB at the quenching temperature of 940°C, while many slender lath bainite and a lot of carbides between the lath appear which easily makes the lath ferrite become a crack propagation path and may produce brittle fracture. The original austenite grain coarsens with the further increase in the temperature. The account of GB structure decreases, while the lamellar bainite ferrite gradually increases with the rising of quenching temperature. The width of the lath increases and the austenite grain boundary gradually becomes clear when improving the quenching. When the temperature reached 980°C, the number of lamellar bainite increases, and the GB structure further decreases. These cancel out the precipitation strengthening of the second-phase particles and the impact property is significantly reduced. The impact energy improves somewhat at the quenching temperature of 1,020°C, although the GB structure is missed and all the bainite is lath. That may be due to the increase in the solid solubility of microalloying elements in the steel at this temperature, where more second-phase particles are precipitated out during the tempering process leading to that the precipitation strengthening effect is greater than the toughness loss caused by grain coarsening. In Figure 7, the overall microstructure hardness of the experimental steel is in an upward trend with the increase in the quenching temperature, which is mainly related to "dispersion hardening" in the tempering process. The increase in quenching temperature leads to an increase in the solid solution content of Ti and Nb in the experimental steel. During tempering, a large amount of hard carbides that increase the micro hardness of the steel is generated in the steel matrix (as shown in Figure 6). As for the temperature between 860 and 900°C, the micro hardness changes only slightly, possibly because only a small amount of carbide dissolution occurs during quenching and holding.

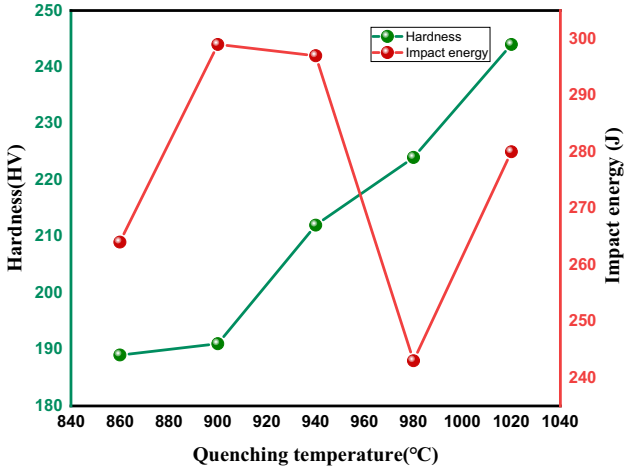

Figure 7: Relationship between mechanical properties of experimental steels and quenching temperature.

4 Conclusion

The thermodynamic precipitation behavior of second-phase particles in Nb-containing high titanium microalloyed steels and its effect on microstructure and properties were systematically investigated. The effects of quenching temperatures on the microstructure and mechanical properties of the experimental steel were studied as well.

(1) In the process of equilibrium cooling the precipitation of the experimental steel, the precipitation order of second phase is $Ti_4C_2S_2$ → FCC_A1#3 → FCC_A1#2 → MnS → Cementite → $M_2P\_C_{22}$ → M_5C_2 → $M_{23}C_6$ → M_7C_3. $Ti_4C_2S_2$ precipitates in the solid–liquid region leading to the inhibition of precipitation of MnS. Thus, MnS precipitates in large quantities in a very small temperature range after decomposition of $Ti_4C_2S_2$. FCC_A1#3 phase is mainly composed of Ti, Nb, C, and N elements, and mainly start to precipitates in the form of Ti(C, N) at the end of solidification (about 1,498°C). FCC_A1#2 is isomorphic with FCC_A1#3 which precipitates mainly in the form of (Ti, Nb)C around 1,266°C, and the content of Ti and Nb elements is much higher than that of FCC_A1#3.

(2) The average austenite grain size of the experimental steel increases exponentially with the increase in the quenching temperature, and the growth rate gradually slows down with the increase in the soaking time. The effect of quenching temperature on grain size is

much greater than that of soaking time. The grain grows up rapidly at the temperature higher than 1,100°C. The average size of austenitic grain is larger than ferrite at the temperature of 1,000°C and soaking time of more than 60 min. Thus, in the actual heat treatment process, the quenching temperature should be controlled below 1,100°C and the soaking time should not exceed 60 min to avoid abnormal grain growth.

(3) The micro hardness of the test steels is significantly increased by the effect of "dispersion hardening", while the impact energy at low temperature fluctuated up and down under the combined action of the precipitation strengthening of the second-phase particles and the loss of strength and toughness due to the change in microstructure, which is still far beyond the control standard.

Acknowledgments: The authors gratefully acknowledge the financial support from the Natural Science Foundation of Hebei Province, China (E2020318006) and Venture & Innovation Support Program for Chongqing Overseas Returnees (cx2019026).

Funding information: The Natural Science Foundation of Hebei Province, China (E2020318006) and the Venture & Innovation Support Program for Chongqing Overseas Returnees, China (cx2019026).

Author contributions: Xiaopei Guo: data curation; formal analysis; investigation; Writing – original draft preparation. Tao Li: supervision; Writing – reviewing and editing. Zhiqiang Shang: formal analysis, Writing – reviewing and editing. Yulin Zhu: Characterization of optical microscope (OM) and scanning electron microscope (SEM). Guannan Li: mechanical testing.

Conflict of interest: The authors declare that they have no known competing financial interests or personal relationships that could have appeared to influence the work reported in this article.

Data availability statement: The raw/processed data are available.

References

[1] Pandit, A., A. Murugaiyan, A. S. Podder, A. Haldar, D. Bhattacharjee, S. Chandra, et al. Strain induced precipitation of complex carbonitrides in Nb–V and Ti–V microalloyed steels. *Scripta Materialia*, Vol. 53, No. 11, 2005, pp. 1309–1314.

[2] Fernández, J., S. Illescas, and J. M. Guilemany. Effect of microalloying elements on the austenitic grain growth in a low carbon HSLA steel. *Materials Letters*, Vol. 61, No. 11, 2007, pp. 2389–2392.

[3] Hong, S. G., H. J. Jun, K. B. Kang, and C. G. Park. Evolution of precipitates in the Nb–Ti–V microalloyed HSLA steels during reheating. *Scripta Materialia*, Vol. 48, No. 8, 2003, pp. 1201–1206.

[4] Bahl, S., A. S. Krishnamurthy, S. Suwas, and K. Chatterjee. Controlled nanoscale precipitation to enhance the mechanical and biological performances of a metastable β Ti-Nb-Sn alloy for orthopedic applications. *Materials & Design*, Vol. 126, 2017, pp. 226–237.

[5] Sozańska-Jędrasik, L., J. Mazurkiewicz, K. Matus, and W. Borek. Effect of Nb solute and NbC precipitates on dynamic or static recrystallization in Nb steels. *Journal of Iron and Steel Research International*, Vol. 19, No. 11, 2012, pp. 52–56.

[6] Monschein, S., M. Kapp, D. Zügner, J. Fasching, A. Landefeld, and R. Schnitzer. Influence of microalloying elements and deformation parameters on the recrystallization and precipitation behavior of two low-alloyed steels. *Steel Research International*, Vol. 92, 2021, id. 2100065.

[7] Charleux, M., W. J. Poole, M. Militzer, and A. Deschamps. Precipitation behavior and its effect on strengthening of an HSLA-Nb/Ti steel. *Metallurgical and Materials Transactions A-Physical Metallurgy and Materials Science*, Vol. 32, No. 7, 2001, pp. 1635–1647.

[8] Kostryzhev, A. G., A. Al Shahrani, C. Zhu, S. P. Ringer, and E. V. Pereloma. Effect of deformation temperature on niobium clustering, precipitation and austenite recrystallisation in a Nb–Ti microalloyed steel. *Materials Science and Engineering: A*, Vol. 581, 2013, pp. 16–25.

[9] Mohebbi, M. S., M. H. Parsa, M. Rezayat, and L. Orovčík. Analysis of flow behavior of an Nb-Ti microalloyed steel during hot deformation. *Metallurgical and Materials Transactions A*, Vol. 49, No. 5, 2018, pp. 1604–1614.

[10] Zhou, C. and R. Priestner. The evolution of precipitates in Nb-Ti microalloyed steels during solidification and post-solidification cooling. *ISIJ International*, Vol. 36, No. 11, 1996, pp. 1397–1405.

[11] Ma, F., G. Wen, and W. Wang. Effect of cooling rates on the second-phase precipitation and proeutectoid phase transformation of a Nb–Ti microalloyed steel slab. *Steel Research International*, Vol. 84, No. 4, 2013, pp. 370–376.

[12] Grajcar, A. Thermodynamic analysis of precipitation processes in Nb–Ti-microalloyed Si–Al TRIP steel. *Journal of Thermal Analysis and Calorimetry*, Vol. 118, No. 2, 2014, pp. 1011–1020.

[13] Türkmen, M., M. A. Erden, H. Karabulut, and S. Gündüz. The effects of heat treatment on the microstructure and mechanical properties of Nb-V microalloyed powder metallurgy steels. *Acta Physica Polonica A*, Vol. 135, No. 4, 2019, pp. 834–836.

[14] Bolanowski, K. Effect of heat treatment on mechanical properties and microstructure morphology of low-alloy high-strength steel. *Archives of Metallurgy and Materials*, Vol. 61, No. 2, 2016, pp. 475–480.

[15] Gao, W. L., Y. Leng, D. F. Fu, and J. Teng. Effects of niobium and heat treatment on microstructure and mechanical properties

of low carbon cast steels. *Materials & Design*, Vol. 105, 2016, pp. 114–123.
[16] Deng, X., Z. Wang, R. D. K. Misra, J. Han, and G. Wang. Precipitation behavior and mechanical properties of Ti-Mo medium-carbon steel during austenite to bainite transformation. *Journal of Materials Engineering and Performance*, Vol. 24, No. 2, 2015, pp. 1072–1078.
[17] Hossain, R., F. Pahlevani, and V. Sahajwalla. Stability of retained austenite in high carbon steel - Effect of post-tempering heat treatment. *Materials Characterization*, Vol. 149, 2019, pp. 239–247.
[18] Li, X. and Y. Wei. Effect of austenitising heat treatment on microstructure and properties of a nitrogen bearing martensitic stainless steel. *Open Physics*, Vol. 17, No. 1, 2019, pp. 601–606.
[19] Li, Z. L., D. Chen, J. Kang, G. Yuan, and G. D. Wang. The effect of heat treatment and precipitation on grain growth of TRIP steel. *Steel Research International*, Vol. 89, 2018, id. 5.
[20] Graux, A., S. Cazottes, D. De Castro, D. San Martín, C. Capdevila, J. M. Cabrera, et al. Precipitation and grain growth modelling in Ti-Nb microalloyed steels. *Materialia*, Vol. 5, 2019, id. 5.
[21] Zhang, J., T. Zhang, and Y. Yang. Microstructure and properties evolution of Nb-bearing medium Cr wear-resistant cast steel during heat treatment. *Journal of Iron and Steel Research International*, Vol. 28, No. 6, 2021, pp. 739–751.
[22] Liang, L., Y. Lixin, L. Guanghui, C. Yi, D. Xiangtao, and W. Zhaodong. Effect of heat treatment on microstructure and mechanical properties of low-alloy wear-resistant steel NM450. *Materials Research Express*, Vol. 8, 2021, id. 4.
[23] Adamczyk-Cieślak, B., M. Koralnik, R. Kuziak, M. Smaczny, T. Zygmunt, and J. Mizera. Effects of heat treatment parameters on the microstructure and properties of bainitic steel. *Journal of Materials Engineering and Performance*, Vol. 28, No. 11, 2019, pp. 7171–7180.
[24] Park, M., K. Kim, J. Jang, H. C. Kim, H. S. Moon, J. B. Jeon, et al. Influence of heat treatment on mechanical properties for cold worked 304 austenitic stainless steel. *Korean Journal of Metals and Materials*, Vol. 56, No. 7, 2018, pp. 490–498.
[25] Hofer, C., S. Primig, H. Clemens, F. Winkelhofer, and R. Schnitzer. Influence of heat treatment on microstructure stability and mechanical properties of a carbide-free bainitic steel. *Advanced Engineering Materials*, Vol. 19, No. 4SI, 2017, id. 1600658.
[26] Hidalgo, J., M. Vittorietti, H. Farahani, F. Vercruysse, R. Petrov, and J. Sietsma. Influence of M23C6 carbides on the heterogeneous strain development in annealed 420 stainless steel. *Acta Materialia*, Vol. 200, 2020, pp. 74–90.
[27] Lewis, M. H. and B. Hattersley. Precipitation of M23C6 in austenitic steels. *Acta Metallurgica*, Vol. 13, No. 11, 1965, pp. 1159–1168.